

This is a repository copy of *Landmark-free, parametric hypothesis tests regarding two-dimensional contour shapes using coherent point drift registration and statistical parametric mapping*.

White Rose Research Online URL for this paper:

<https://eprints.whiterose.ac.uk/173432/>

Version: Accepted Version

Article:

Pataky, Todd, Yagi, Masahide, Ichihashi, Noriaki et al. (1 more author) (2021) Landmark-free, parametric hypothesis tests regarding two-dimensional contour shapes using coherent point drift registration and statistical parametric mapping. PeerJ Computer Science. e542. ISSN 2376-5992

<https://doi.org/10.7717/peerj-cs.542>

Reuse

This article is distributed under the terms of the Creative Commons Attribution (CC BY) licence. This licence allows you to distribute, remix, tweak, and build upon the work, even commercially, as long as you credit the authors for the original work. More information and the full terms of the licence here:

<https://creativecommons.org/licenses/>

Takedown

If you consider content in White Rose Research Online to be in breach of UK law, please notify us by emailing eprints@whiterose.ac.uk including the URL of the record and the reason for the withdrawal request.

1 Landmark-free, parametric hypothesis tests 2 regarding two-dimensional contour shapes 3 using coherent point drift registration and 4 statistical parametric mapping

5 Todd C. Pataky¹, Masahide Yagi¹, Noriaki Ichihashi¹, and Philip G. Cox^{2,3}

6 ¹Department of Human Health Sciences, Kyoto University Graduate School Of Medicine,
7 Kyoto, Japan

8 ²Department of Archaeology, University of York, York, UK

9 ³Hull York Medical School, University of York, York, UK

10 Corresponding author:

11 Todd C. Pataky¹

12 Email address: pataky.todd.2m@kyoto-u.ac.jp

13 ABSTRACT

14 This paper proposes a computational framework for automated, landmark-free hypothesis testing of 2D
15 contour shapes (i.e., shape outlines), and implements one realization of that framework. The proposed
16 framework consists of point set registration, point correspondence determination, and parametric full-
17 shape hypothesis testing. The results are calculated quickly (<2 s), yield morphologically rich detail
18 in an easy-to-understand visualization, and are complimented by parametrically (or nonparametrically)
19 calculated probability values. These probability values represent the likelihood that, in the absence of
20 a true shape effect, smooth, random Gaussian shape changes would yield an effect as large as the
21 observed one. This proposed framework nevertheless possesses a number of limitations, including
22 sensitivity to algorithm parameters. As a number of algorithms and algorithm parameters could be
23 substituted at each stage in the proposed data processing chain, sensitivity analysis would be necessary
24 for robust statistical conclusions. In this paper, the proposed technique is applied to nine public datasets
25 using a two-sample design, and an ANCOVA design is then applied to a synthetic dataset to demonstrate
26 how the proposed method generalizes to the family of classical hypothesis tests. Extension to the analysis
27 of 3D shapes is discussed.

28 INTRODUCTION

29 The statistical analysis of shape variation is relevant to a wide variety of academic fields including:
30 evolutionary biology (Mitteroecker and Gunz, 2009), biomechanics (Pedoia et al., 2017), computer vision
31 (Murphy-Chutorian and Trivedi, 2008), and many others (Da Costa and Cesar, 2000; Rohlf and Marcus,
32 1993; Adams et al., 2004, 2013). A key methodological framework for the statistical analysis of shape to
33 have emerged in the literature is Geometric Morphometrics (Corti, 1993; Bookstein, 1996; Slice, 2007;
34 Zelditch et al., 2012). Geometric Morphometrics consists of a variety of statistical techniques, ranging
35 from classical hypothesis testing (e.g. Goodall, 1991) and classical dimensionality reduction techniques
36 like principal component analysis (Adams et al., 2004) to machine learning techniques like unsupervised
37 clustering (Renaud et al., 2005). This paper is concerned primarily with classical hypothesis testing as it
38 pertains to shape analysis.

39 A common geometric morphometric approach to classical hypothesis testing regarding group differ-
40 ences (depicted in Fig. 1a), consists of: (1) landmark definition, (2) spatial registration, and (3) Procrustes
41 ANOVA (Goodall, 1991). Landmark definition refers to the manual identification and digitizing (i.e.,
42 XYZ coordinate specification) of homologous points on multiple objects, for example the corners on
43 polyhedra. Spatial registration refers to the optimal, non-shearing affine alignment of a set of landmarks;
44 that is, the optimal translation, rotation and scaling of each set of landmarks is calculated so that the

45 the landmarks are optimally aligned in space. Procrustes ANOVA is effectively equivalent to classical
46 ANOVA, where Procrustes distance is the dependent variable (Zelditch et al., 2012).

47 Landmarks with evolutionary, developmental or functional homology are essential for accurate
48 interpretation of results (Hallgrímsson et al., 2015), especially for biological studies which seek to
49 understand morphological variation in the context of evolution (e.g. Stayton, 2005; Morgan, 2009;
50 Casanovas-Vilar and Van Dam, 2013; Dumont et al., 2016; Page and Cooper, 2017), ontogeny (e.g.
51 Klingenberg and McIntyre, 1998; Mitteroecker et al., 2004; Singleton, 2015) or function (e.g. Terhune
52 et al., 2015; Toro-Ibacache et al., 2016). A key practical advantage of landmark approaches is that
53 they impose problem tractability; they convert abstract, usually high-dimensional shape representations
54 including images, scans and line contours, to a relatively small set of numeric coordinates which can be
55 assembled into readily processable data formats like text files and spreadsheets. This practical advantage
56 is reinforced by well-established statistical theory (e.g. Gower, 1975; Kendall, 1977, 1984, 1985; Kent,
57 1994; Rohlf, 1999) which describes a comprehensive solution for dealing with shape data's inherent
58 dimensionality problem (Rohlf, 2000b,a; Collyer et al., 2015).

59 A common approach to landmark-based hypothesis testing is Procrustes ANOVA. While landmark
60 data themselves are multivariate (i.e., multiple landmarks, each with multiple coordinates are used to
61 describe a single shape), Procrustes ANOVA uses a univariate metric (Procrustes distance) to test shape-
62 relevant hypotheses. One problem with this approach is that a single value is likely inadequate to fully
63 characterize shape effects. Many other shape descriptors exist (Kurnianggoro et al., 2018), including both
64 univariate metrics like eccentricity and multivariate metrics like geometric moments (Zhang and Lu, 2004).
65 It has been argued that focus on relatively low dimensional shape metrics like these is necessary in order
66 to achieve suitable statistical power, with the assumption that too many variables relative to the number of
67 phenotypes can preclude hypothesis testing via parametric methods, especially for small samples (Collyer
68 et al., 2015); one aim of this paper is to challenge that assertion, and to show that hypothesis testing is
69 indeed possible for even high-dimensional representations of shape, and with suitably high statistical
70 power for even relatively small sample sizes.

71 A related sample size-relevant theoretical limitation of Procrustes ANOVA is that there is no known
72 parametric solution to the underlying Procrustes distance probability distributions. Consequently, sta-
73 tistical inference is conducted nonparametrically, often using bootstrapping or permutation techniques
74 (Zelditch et al., 2012, pp.248-259). These nonparametric procedures are inherently poor for small sample
75 sizes (Anderson and Braak, 2003; Brombin and Salmaso, 2009) because the probability distributions are
76 constructed empirically and numerically, using the actual data, and both the precision and accuracy of
77 these nonparametrically constructed distributions can decrease substantially with small sample sizes.

78 A variety of landmark-free or landmark-minimal methods also exist, including for example techniques
79 that fit mathematical curves to shape outlines (Rohlf, 1990). One technique that has been particularly
80 widely used is elliptical Fourier analysis (Claude, 2013; Bonhomme et al., 2014), which considers the
81 spatial relations amongst neighboring points, and characterizes the spatial frequencies along the contour
82 perimeter as a change-relevant representation of shape. Elliptical Fourier analysis has been frequently
83 employed to analyse structures on which few homologous landmarks can be identified such as fins, jaws
84 and teeth (e.g. Fu et al., 2016; Hill et al., 2018; Cullen and Marshall, 2019). These methods are highly
85 relevant to the methods described in this paper, in that they deal with original, high-dimensional shape
86 data like 2D contours and 3D surface scans.

87 While landmark-free or landmark-minimal methods initially operate on original high-dimensional
88 shape data, they tend to use much lower-dimensional representations of shape when conducting classical
89 hypothesis testing. For example, elliptical Fourier analysis tends to conduct hypothesis testing using
90 a relatively small number (fewer than ten) harmonic coefficients (Bonhomme et al., 2014). Common
91 landmark and landmark-free methods are thus similar from from a hypothesis testing perspective in that
92 the hypothesis tests ultimately pertain to relatively low-dimensional shape metrics.

93 This main aim of this paper was to show that classical hypothesis testing is possible on original, high-
94 dimensional shape data, and in particular on continuous surfaces, without the need for low-dimensional
95 shape representations, and with suitably high power even for analyses of relatively small samples. The
96 methodology, which we refer to as 'continuous, mass-multivariate analysis' consists of a number of
97 previously described techniques including: (1) point set registration, (2) correspondence, and (3) mass-
98 multivariate hypothesis testing. This combination of techniques allows one to conduct landmark-free
99 hypothesis testing on original surface shapes. For interpretive convenience we limit focus to 2D contours

100 (Bookstein, 1997; Carlier et al., 2016), but in the Discussion describe how the proposed methodology can
 101 be applied to 3D surfaces.

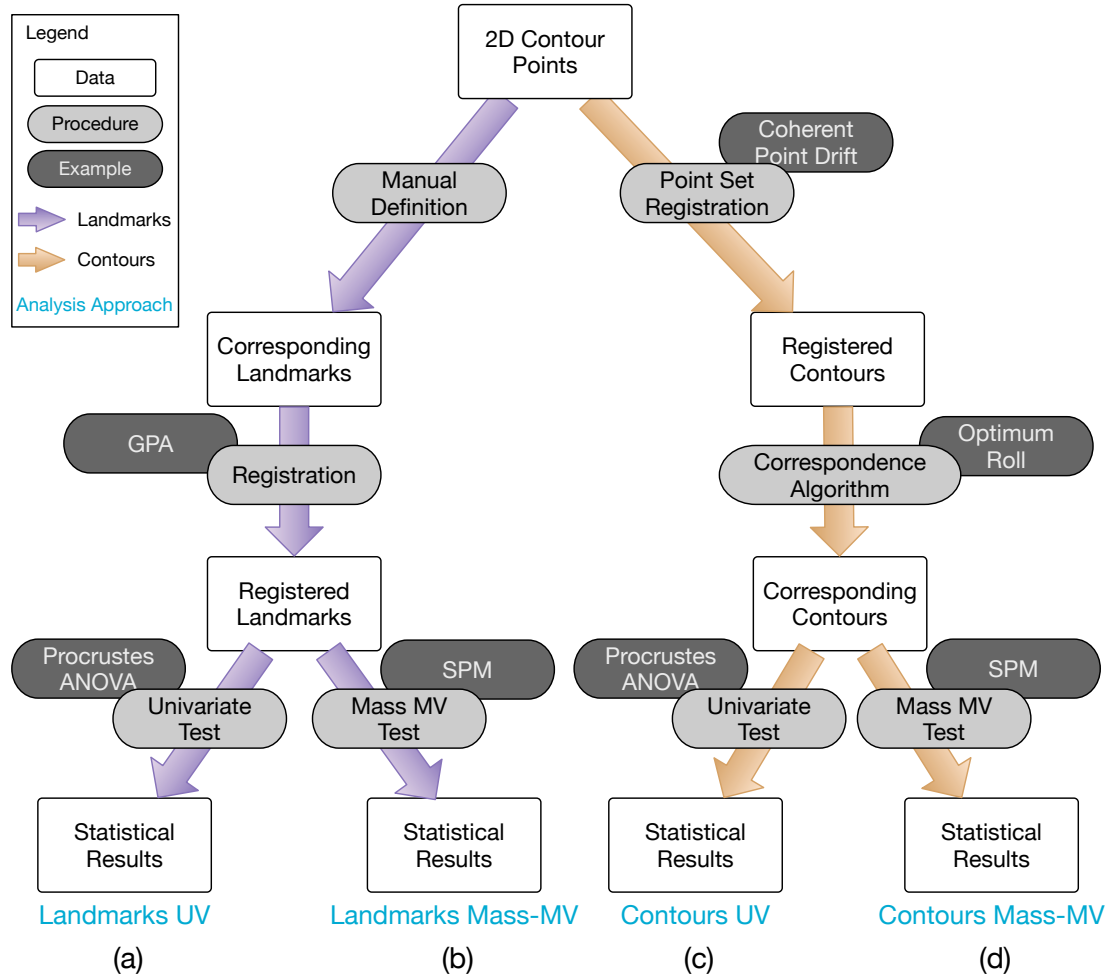


Figure 1. Overview of 2D contour data processing approaches employed in this paper. (a) The most common analysis approach, consisting of Generalized Procrustes Analysis (GPA) and Procrustes ANOVA for landmarks. (b) Same as (a), but using mass-multivariate (MV) analysis instead of Procrustes ANOVA’s univariate (UV) approach. (c) and (d) are conceptually equivalent to (a) and (b), respectively, but operate on full contour data instead of landmark data, and can also be fully algorithmic. Statistical Parametric Mapping (SPM) is a methodology for mass-MV analysis of continuous data. See text for more details.

METHODS

Analyses were conducted in Python 3.6.10 (van Rossum, 2019) using Anaconda 3.6.10 (Anaconda, 2020) and in R 3.6.2 (R Core Team, 2019). Data processing scripts are available along with all original and processed data in this project’s public repository at: <https://github.com/0todd0000/lmfree2d>.

Datasets

Nine datasets were analyzed (Fig.2). All datasets were taken from the the open-source 2D Shape Structure database (Carlier et al., 2016) (<http://2dshapesstructure.github.io>). The database consists of 70 different shape classes. Inclusion criteria for shape class were: (i) qualitatively similar geometry in at least 10 shapes (Fig.3), and (ii) at least four readily identifiable landmarks for all contour shapes.

Each dataset consisted of 20 contour shapes, where a ‘dataset’ represents a shape class (e.g., ‘Bell’ or ‘Face’) and individual shapes represent morphological variation within that shape class. We manually selected ten shapes from each dataset in a pseudo-random manner in order to span a range of effect sizes; in the Results, note that p values span a wide range ($p < 0.001$ to $p > 0.9$). We selected just ten shapes primarily because it has been suggested that parametric procedures are unsuitable for the morphological analyses of small samples (Collyer et al., 2015), and we wished to demonstrate that the proposed parametric technique is indeed sufficiently powerful for small-sample analyses. Secondary reasons for considering just 10 shapes included: (1) qualitatively different within-class geometry, implying that statistical comparisons would be dubious if all 20 shapes were used, (2) inconsistent curvature characteristics (e.g., some with sharp corners, others with no discernible corners), implying landmarking difficulties, and (3) untrue contour data (e.g., internal loops and thus non-convex polygons) implying that contour parameterization was not possible for all shapes.

Two-sample tests were conducted on each dataset using the four approaches as described below. For replicability, the final set of ten shapes selected for analysis from each class are redistributed in this project’s repository at: <https://github.com/0todd0000/lmfree2d>. Note that the ultimately selected contours had a variable number of contour points within each dataset (Table 1).

Table 1. Dataset count summary. Point counts refer to the original data from Carlier et al. (2016).

Name	Shapes	Points			Landmarks
		Min	Median	Max	
Bell	10	101	104	185	8
Comma	10	101	104	108	4
Device8	10	101	104	107	8
Face	10	103	104	106	4
Flatfish	10	100	102	112	5
Hammer	10	102	105	119	7
Heart	10	102	105	109	4
Horseshoe	10	106	109	128	6
Key	10	103	106	115	5

Data processing

The 2D contour shape data were analyzed using four related approaches, consisting of the four combinations of (i) landmarks vs. contours, and (ii) univariate (UV) vs. mass-multivariate (mass-MV). These four approaches are summarized in Fig.1. The Landmarks-UV approach (Fig.1a) is common in the literature, none of the other approaches is common. The primary purpose of this study was to compare and contrast the Landmarks-UV and Contours-MassMV approaches (Fig.1a,d). We also employed intermediary approaches (Fig.1b,c) to more clearly highlight the differences between the two main approaches.

Landmarks univariate (UV) analysis

Landmarks were defined for each dataset as depicted in Fig.2. Both the number of landmarks (Table 1) and their locations were selected in an *ad hoc* manner, with the qualitative requirement of readily

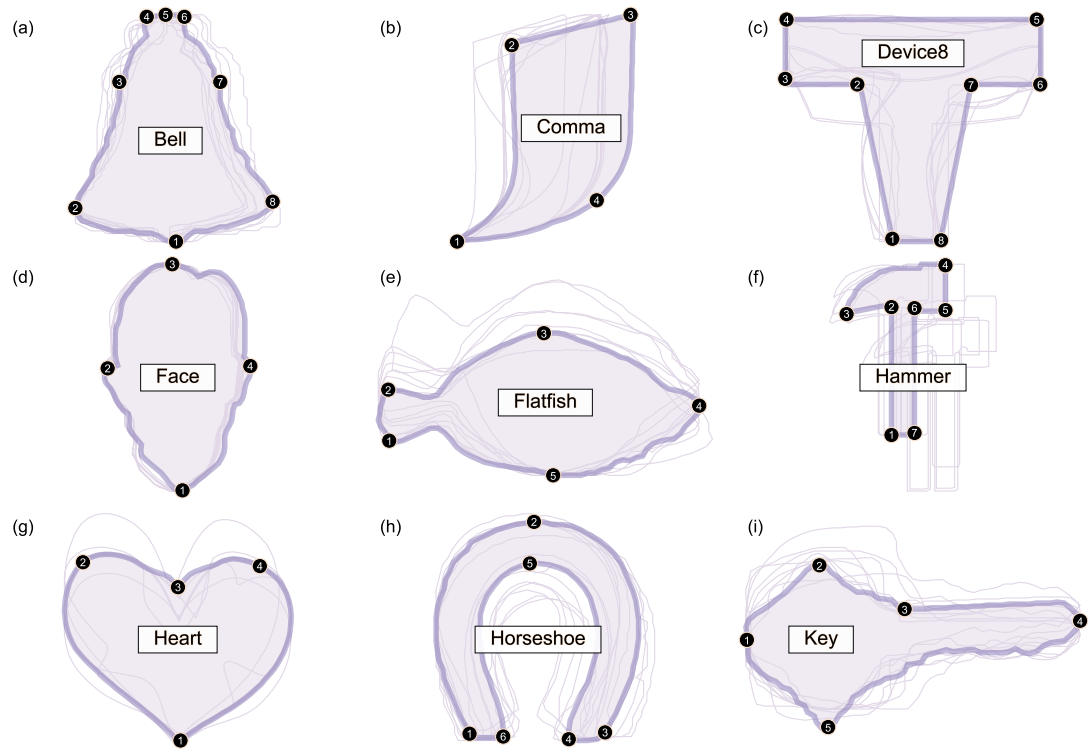


Figure 2. Overview of analyzed datasets. All contour data are available in the 2D Shape Structure Dataset (Carrier et al., 2016). For each dataset in this figure, one representative shape is highlighted, along with its numbered landmarks. Note that shape variance ranges from relatively small (e.g. Bell, Face) to relatively large (e.g. Device8, Heart).

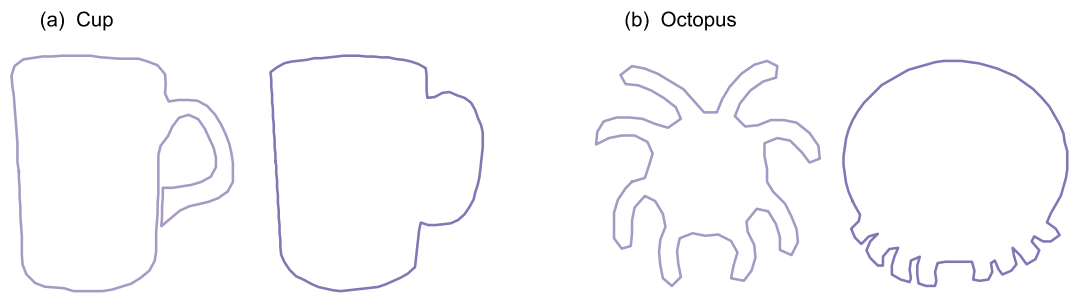


Figure 3. Shape class exclusion examples. Shape classes were excluded if they contained shapes with qualitatively different contour geometry. For example: (a) the ‘cup’ class was excluded because some shapes had unattached handles with holes and others had attached handles without holes. (b) The ‘octopus’ class was excluded because the eight appendages appeared in non-homologous locations.

139 identifiable, homologous locations. The ultimately selected landmarks arguably span a representative
 140 range of landmarking possibilities.

141 One operator used a mouse to manually digitize the landmarks for each of the 90 shapes (10 shapes
 142 for each of 9 datasets). The operator was ignorant of the final shape groupings for the ultimate two-sample
 143 tests (see below), implying that the landmarking was performed without grouping bias.

144 The landmarks were spatially registered using Generalized Procrustes Analysis (GPA) (Gower, 1975),
 145 and the resulting registered landmarks were analyzed in a univariate manner, using Procrustes ANOVA

146 (Goodall, 1991) — a method which considers the variance in the Procrustes distance across a dataset.
 147 Note that the Procrustes distance is a scalar quantity that summarizes shape difference, and thus that this
 148 method is univariate. GPA and Procrustes ANOVA were both conducted using the **geomorph** package for
 149 R (Adams and Otárola-Castillo, 2013).

150 **Landmarks mass-multivariate (mass-MV) analysis**

151 This approach was identical to the Landmarks-UV approach described above, except for statistical analysis.

152 The two-sample Hotelling's T^2 statistic was calculated for each landmark according to its definition:

$$T_i^2 = \frac{n_1 n_2}{n_1 + n_2} (\bar{r}_{1i} - \bar{r}_{2i})^\top W_i^{-1} (\bar{r}_{1i} - \bar{r}_{2i}) \quad (1)$$

153 where i indexes landmarks, the subscripts "1" and "2" index the two groups, n is sample size, \bar{r}_i is the
 154 mean position vector of landmark i , and W_i is the pooled covariance matrix for landmark i :

$$W_i = \frac{1}{n_1 + n_2 - 2} \left(\sum_{j=1}^{n_1} (r_{1ij} - \bar{r}_{1i})(r_{1ij} - \bar{r}_{1i})^\top + \sum_{j=1}^{n_2} (r_{2ij} - \bar{r}_{2i})(r_{2ij} - \bar{r}_{2i})^\top \right) \quad (2)$$

155 where the i index is dropped for convenience in Eqn.2.

156 Statistical inference was conducted in a mass-multivariate manner, using Statistical Parametric
 157 Mapping (SPM) (Friston et al., 2007). SPM bases statistical inferences on the distribution of the maximum
 158 T^2 value (T_{\max}^2), which can be roughly interpreted as the largest landmark effect, and which is defined as:

$$T_{\max}^2 \equiv \max_{i \in L} T_i^2 \quad (3)$$

159 where L is the number of landmarks.

160 SPM provides a parametric solution to the distribution of T_{\max}^2 under the null hypothesis, so significance
 161 can be assessed by determining where in this distribution the observed T_{\max}^2 lies. Classical hypothesis
 162 testing involves the calculation of a critical threshold $(T^2)_{\text{critical}}$, defined as the $(1 - \alpha)$ th percentile of this
 163 distribution, and all landmarks whose T^2 values exceed $(T^2)_{\text{critical}}$ are deemed significant at a Type I error
 164 rate of α . This is a correction for multiple comparisons (i.e., across multiple landmarks) that is 'mass-
 165 multivariate' in the following sense: 'mass' refers to a family of tests, in this case a family of landmarks,
 166 and 'multivariate' refers to a multivariate dependent variable, in this case is a two-component position
 167 vector. This is similar to traditional corrections for multiple comparisons like Bonferroni corrections,
 168 with one key exception: rather than using the total number of landmarks L as the basis for the multiple
 169 comparisons correction, as the Bonferroni correction does, SPM instead solves the mass-MV problem
 170 by assessing the correlation amongst neighboring landmarks or semilandmarks, and using the estimated
 171 correlation to provide a less severe correction than the Bonferroni correction, unless there is no correlation,
 172 in which case the SPM and Bonferroni corrections are equivalent.

173 **Contours univariate (UV) analysis**

174 Similar to the Landmarks UV approach, this approach ultimately conducted Procrustes ANOVA, but
 175 did so on contour data rather than landmark data. This was achieved through two main processing
 176 steps: coherent point drift (CPD) point set registration (Fig.4) and optimum roll correspondence (Fig.5).
 177 Coherent point drift (CPD) (Myronenko and Song, 2010) is a point set registration algorithm that spatially
 178 aligns to sets of points that belong to the same or a similar object. Neither an equal number of points nor
 179 homologous points are required (Fig.4), making this approach useful for contours that have an arbitrary
 180 number of points.

181 Since contour points from arbitrary datasets may generally be unordered (Fig.5a), we started our
 182 analyses by randomly ordering all contour points, then applying CPD to the unordered points. We
 183 acknowledge that many 2D contour datasets consist of ordered points — including those in the database
 184 used for this study (Carlier et al., 2016) — but since 3D surface points are much more likely to be
 185 unordered, we regard unordered point support as necessary for showing that the proposed method is
 186 generalizable to 3D analyses. Following CPD, we re-ordered the points using parametric surface modeling

187 (Bingol and Krishnamurthy, 2019), which fits a curved line to the contour, and parameterizes the contour
188 using position u , where u ranges from zero to one (Fig.6). This contour parameterization results in a
189 continuous representation of the contour, from which an arbitrary number of ordered points (Fig.5b) can
190 be used to discretize the contour of each shape for subsequent analysis. We used NURBS parameterization
191 with B-spline interpolation (Bingol and Krishnamurthy, 2019) to calculate specific contour point locations.
192 We then applied an optimum roll transformation, which found the value of u for one contour that minimized
193 the deformation energy across the two contours (Fig.5c,d).

194 We repeated contour parameterization, ordering, and optimum roll correspondence across all contour
195 shapes, using the shape with the maximum number of contour points in each dataset as the template shape
196 to which the nine other shapes were registered. **Note that this registration procedure is unrelated to the**
197 **traditional landmark analyses described in ‘Landmark UV analysis’ above, for which an equal number of**
198 **points is a requirement of registration and analysis. The correspondence analysis step resulted in an equal**
199 **number of contour points, upon which we conducted Procrustes ANOVA.**

200 **Contours mass-multivariate (mass-MV) analysis**

201 This approach was identical to the Contours-UV approach, with the exception of statistical analysis, which
202 we conducted using SPM as outlined above. Unlike the landmark data above, which are generally spatially
203 disparate, contour points are spatially proximal, and neighboring points tend to displace in a correlated
204 manner. For example, if one contour point in a specific shape lies above the mean point location, its
205 immediate neighbors also tend to lie above the mean location). SPM leverages this correlation to reduce
206 the severity of the multiple comparisons correction, and SPM solutions converge to a common $(T^2)_{\text{critical}}$
207 regardless of the number of contour points, provided the number of contour points is sufficiently large
208 to embody the spatial frequencies of empirical interest, as outlined in classical signal processing theory
209 (Nyquist, 1928).

210 As SPM uses parametric inference to calculate the critical T^2 threshold, and Procrustes ANOVA uses
211 nonparametric inference, we also conduct Contours Mass-MV analysis using statistical non-parametric
212 mapping (Nichols and Holmes, 2002), which uses permutation to numerically build the T^2_{max} distribution
213 under the null hypothesis. This permutation approach converges to the parametric solution when the
214 residuals are normally distributed (i.e., point location variance follows an approximately bivariate Gaussian
215 distribution). All SPM analyses were conducted in **spm1d** (Pataky, 2012); note that one-dimensional
216 SPM is sufficient because the contour domain (U) is one-dimensional (Fig.6).

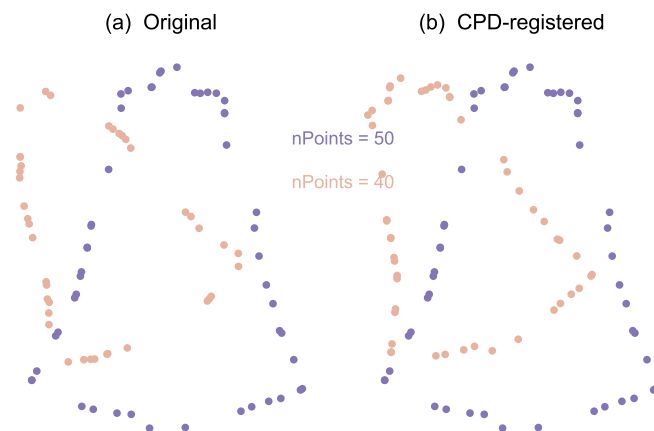


Figure 4. Example point set registration using the coherent point drift (CPD) algorithm (Myronenko and Song, 2010). Note that CPD requires neither corresponding points, nor an equal number of points.

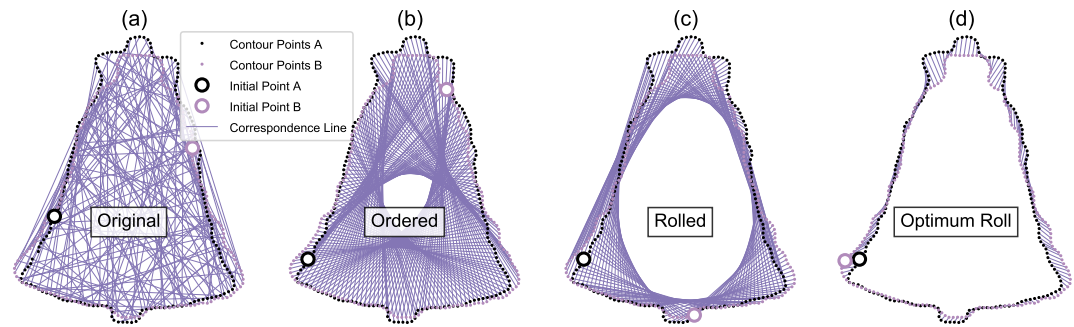


Figure 5. Example optimum roll correspondence. (a) Original data, consisting of an equal number of contour points, arranged in a random order. (b) Ordered points; clockwise along the contour. (c) Rolled points; moving the initial point of contour B brings the shapes into better correspondence. (d) Optimally rolled points; the total deformation energy across all points (i.e. the sum-of-squared correspondence line lengths) is minimum.

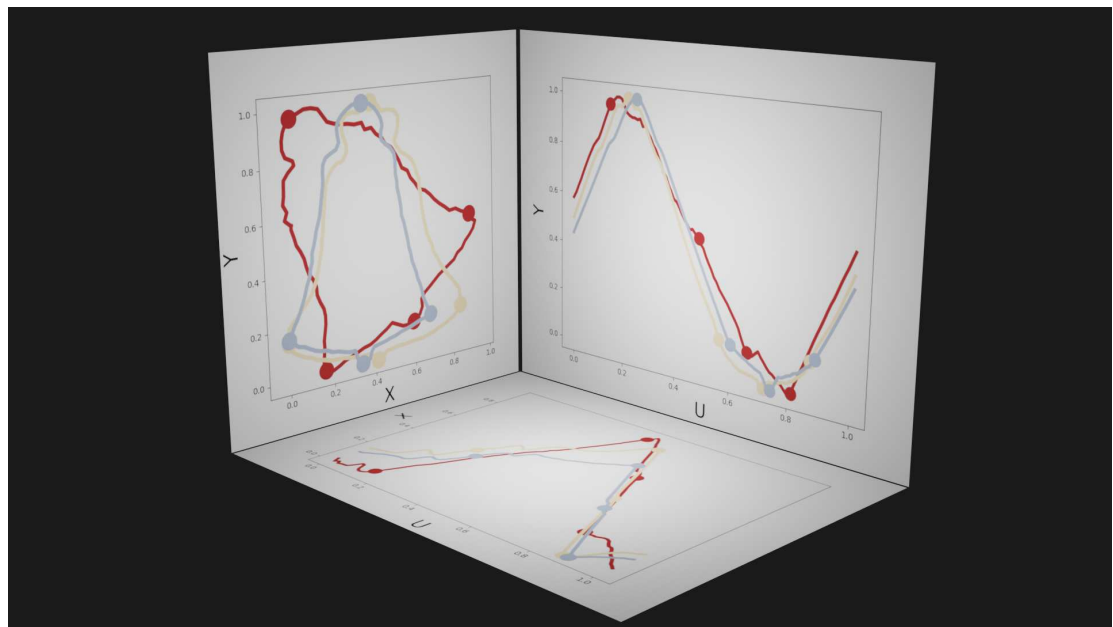


Figure 6. Example parametric representations of 2D contour shape. Dots represent manually defined landmarks, and are shown as visual references. Left panel (XY plane): the spatial plane in which shape data are conventionally presented. The three colors represent different shapes. Bottom panel (UX plane) and right panel (UY plane): abstract planes in which U represents the parametric position (from 0 to 1) along the contour; positions $U=0$ and $U=1$ are equivalent.

217 **RESULTS**

218 The four analyses approaches produced a range of p values from very low ($p < 0.001$) to very high
 219 ($p > 0.9$), and even yielded a large range of p values for single datasets (e.g. Heart: $0.016 < p < 0.940$)
 220 (Table 2). Of the nine datasets, only two yielded consistent hypothesis testing conclusions (at $\alpha = 0.05$)
 221 across the four analysis approaches: for the Comma dataset all approaches failed to reject the null
 222 hypothesis, and for the Flatfish dataset all approaches rejected the null hypothesis. The seven other
 223 datasets showed a range of disagreement on the methods. For example, for the Key dataset neither
 224 Landmarks approach reached significance, but both Contours approaches did reach significance. For
 225 the Hammer dataset, three approaches failed to reach significance, but the Contours Mass-MV approach
 226 produced a very low p value ($p < 0.001$). The Landmarks approaches executed comparatively rapidly
 227 (50 ms) compared to the Contours approaches (2 s) (Table 3).

228 Since Procrustes ANOVA results are commonly used in the literature, and are summarized for the
 229 current study in (Table 2), the remainder of the results considers the Mass-MV approaches' results.
 230 First, the Landmarks Mass-MV approach indicate a wide range of T^2 statistic values at each landmark
 231 (Fig,7). For example, Landmark 5 in the Horseshoe dataset (Fig.2) had a very high T^2 value, and all other
 232 landmarks had comparatively low p values (Fig,7). This suggests that (a) shape differences can be highly
 233 localized, and that (b) univariate methods that employ an overall shape change metric, like Procrustes
 234 ANOVA, may not be able to detect these changes, even when the landmarks are identical (Table 2).

235 The Contour Mass-MV results showed little qualitative difference between parametric and non-
 236 parametric inference (Fig.8), with minor exceptions regarding specific locations and spatial extent of
 237 supra-threshold contour points (e.g. Key, Horseshoe). Since this Contour Mass-MV approach is sensitive
 238 to point-specific variation, it was generally more sensitive at detecting changes, as shown in the relatively
 239 high rate of null hypothesis rejection relative to the other approaches (Table 2); that is, even though the
 240 Contours-UV and Contours Mass-MV approaches consider the same data, the latter reached significance
 241 more often than the former, implying that it is more sensitive to location-specific effects. Whether this
 242 sensitivity is a benefit or not is considered in the Discussion.

Table 2. Statistical results summary, probability values. As nonparametric inference yielded similar p values (see Results), only parametric p values are reported in this table for brevity.

Name	Landmarks		Contours	
	UV	Mass-MV	UV	Mass-MV
Bell	0.130	0.302	0.084	0.041
Comma	0.155	0.294	0.719	0.327
Device8	0.022	0.214	0.433	0.681
Face	0.025	0.103	0.052	0.013
Flatfish	0.023	0.016	0.026	0.001
Hammer	0.708	0.206	0.417	< 0.001
Heart	0.940	0.976	0.544	0.016
Horseshoe	0.084	0.008	0.006	0.001
Key	0.532	0.270	0.013	0.022

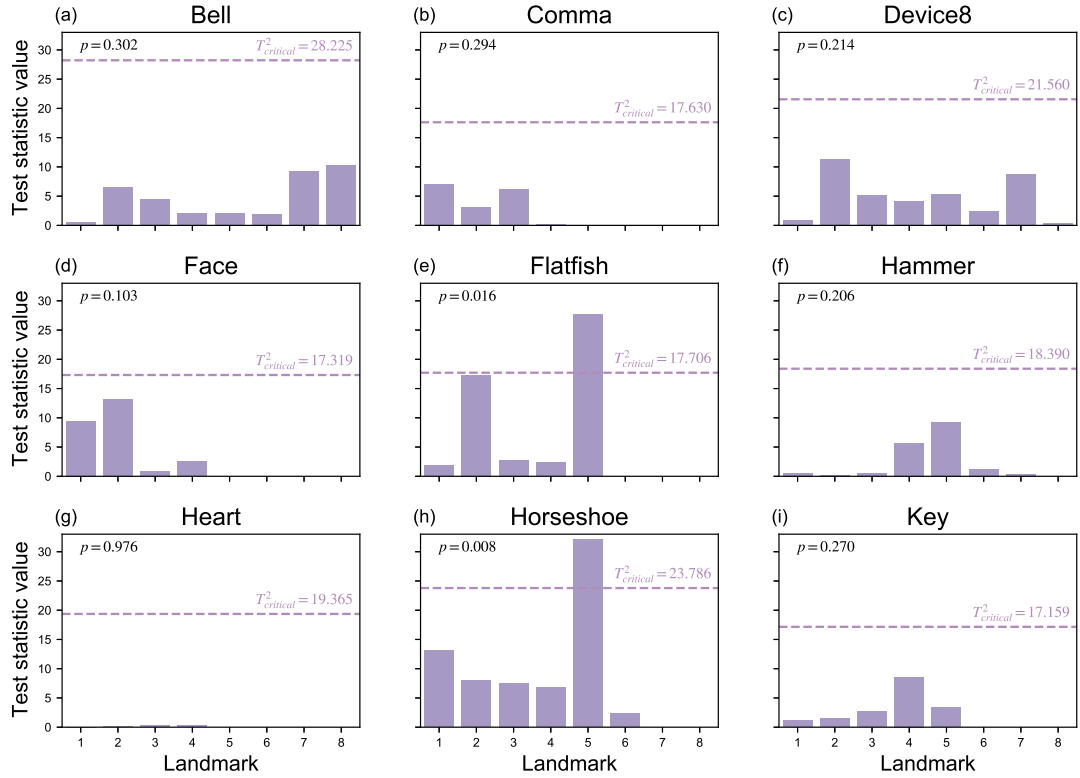


Figure 7. Landmark results from mass-multivariate testing. Landmark-specific T^2 values are presented along with the critical threshold at $\alpha=0.05$, and probability values for the overall mass-multivariate test.

Table 3. Execution durations (unit: ms). Averages across the nine datasets. Procrustes ANOVA (Proc-ANOVA) involved 1000 iterations for each dataset. Average SnPM durations (not shown in this table) were 344.0 and 6336.0 ms for Landmarks Mass-MV and Contours Mass-MV, respectively.

Category	Procedure	Landmarks		Contours	
		UV	Mass-MV	UV	Mass-MV
Registration	CPD	-	-	414.1	414.1
	Point Ordering	-	-	327.9	327.9
	Interpolation	-	-	835.1	835.1
	Correspondence	-	-	40.9	40.9
	GPA	6.7	6.7	8.5	-
Hypothesis test	Proc-ANOVA	60.0	-	99.0	-
	SPM	-	39.3	-	66.8
Total		66.7	46.0	1725.5	1684.8

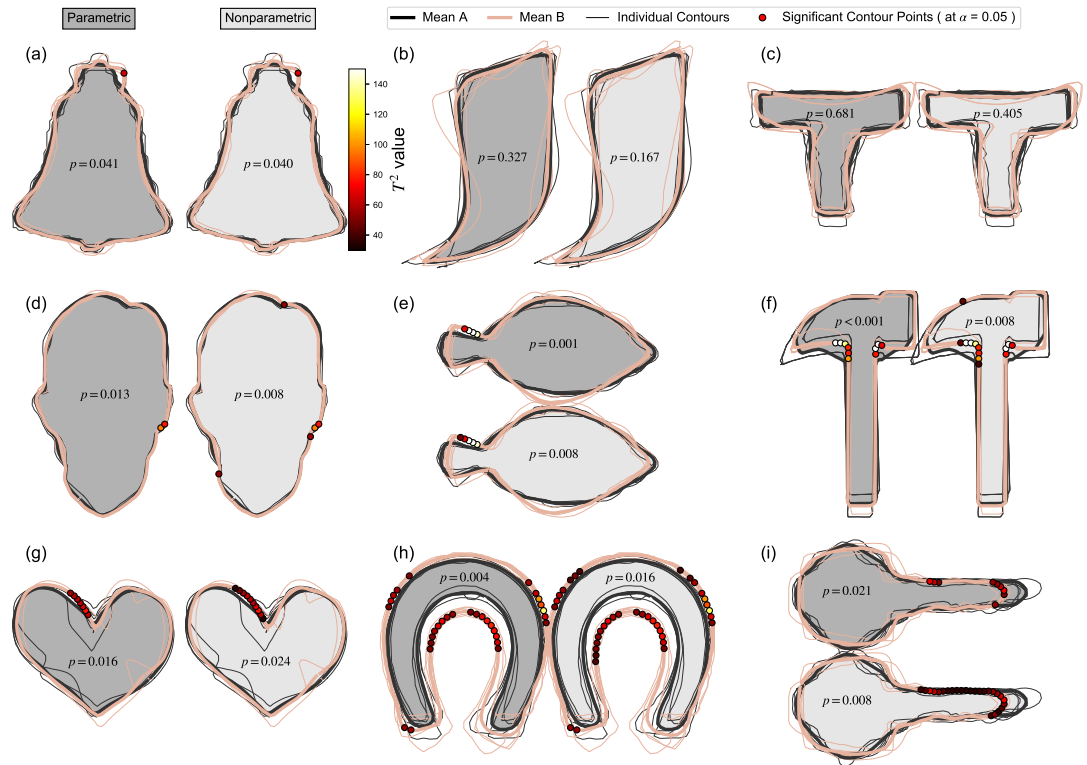


Figure 8. Contours mass-multivariate results using Statistical Parametric Mapping (SPM). Results for both parametric and nonparametric inference are shown. P values represent the probability that random variation in the Mean A contour would produce a deformation as large as in the observed Mean B, given the estimated contour variance. Dots on the Mean B contour represent contour points whose T^2 values exceeded the threshold for significance at $\alpha=0.05$; if the maximum T^2 value did not reach this threshold, the p value is greater than α , and no dots are shown.

243 DISCUSSION

244 Main findings

245 This study's main result is the demonstration that it is possible to conduct fully automated, landmark-free,
246 parametric hypothesis testing regarding whole 2D contour shapes, irrespective of the number of points
247 and point ordering in the original contour data. These analyses can be executed relatively quickly; the
248 current non-optimized implementation required less than 2 s for all analysis steps (Table 3). The proposed
249 analysis framework (Fig.1d) consists of families of previous techniques including: point set registration
250 (e.g. Myronenko and Song, 2010), point correspondence algorithms (e.g. Loy et al., 2000; Myronenko and
251 Song, 2010), and mass-multivariate testing (Friston et al., 2007; Taylor and Worsley, 2008; Chung et al.,
252 2010), and some of these techniques have been used for classical hypothesis testing regarding shapes
253 in the past (Taylor and Worsley, 2008; Chung et al., 2010). A variety of landmark-free techniques have
254 also been previously proposed (e.g. Wuhrer et al., 2011; Taylor and Worsley, 2008; Chung et al., 2010)
255 Nevertheless, these techniques have not, to our knowledge, been previously combined into a general
256 hypothesis testing framework — from raw data to statistical results — as depicted in Fig.1d. The main
257 novelty of this paper is thus the demonstration that it is possible to fully automate data processing from
258 raw 2D contour data to final hypothesis testing results.

259 The second main novelty of this paper is the demonstration that parametric hypothesis testing is
260 possible when conducted at the whole-contour level. We stress that 'possible' implies neither 'valid'
261 nor 'appropriate'; demonstrating the validity and appropriateness of the proposed method would require
262 substantial empirical efforts over a range of datasets, data modalities, experimental designs, and appli-
263 cations, in addition likely to simulation studies, and as such assessing validity and appropriateness are
264 beyond the scope of this paper. We also stress that 'possible' does not imply that one should use the
265 proposed technique in isolation. We believe that the proposed technique offers unique information that is
266 complimentary to other techniques, and that ideally the results of multiple analysis techniques should be
267 corroborated to build interpretive robustness.

268 The proposed analysis framework (Fig.1d) offers various improvements over landmark analysis
269 (Fig.1a) including: (1) the modeling flexibility of classical hypothesis testing, (2) increased objectivity
270 due to avoidance of subjective landmark definition and selection, (3) increased speed due to avoidance
271 of manual work, and (4) unique, implicit morphological meaning in hypothesis testing results. We
272 acknowledge that each of these improvements also involve limitations, and we address these limitations
273 below. We stress that 'objectivity' implies none of 'accurate', 'useful' or 'interpretable'. We use 'objective'
274 instead primarily to mean 'algorithmic'.

275 Statistical Parametric Mapping (SPM)

276 SPM, like most parametric tests, assumes normality, so in this case SPM assumes that the spatial variability
277 of all contour points are distributed in a bivariate Gaussian manner. This distributional assumption could be
278 directly tested using distributional tests in a point-by-point manner. In this paper, instead of directly testing
279 for distributional adherence, we instead tested the assumption indirectly, by conducting nonparametric tests
280 (Fig.8), which do not assume bivariate normality. In this case there were minor quantitative differences
281 between the parametric and nonparametric results, but overall the qualitative interpretations were largely
282 unaffected by the use of parametric vs. nonparametric analysis. This represents relatively strong (albeit
283 indirect) evidence that the parametric approach's distributional assumptions are appropriate at best, or
284 largely inconsequential at worst, for these particular datasets. This however does not **imply** that parametric
285 inference is appropriate for all datasets, so distributional assumptions should generally be tested for all
286 datasets, possibly indirectly through nonparametric tests like those conducted in this paper.

287 Although this paper considered only two-sample tests, SPM supports all classical hypothesis testing
288 procedures, ranging from simple linear regression to MANCOVA (Friston et al., 2007), thereby making
289 the proposed framework highly flexible to arbitrary experimental designs. To emphasize this point, and
290 how it may be valuable for general shape analysis, we conducted a set of supplementary analyses using
291 synthetic data involving simple, circular shapes with controlled morphological effects (Fig.9a,b). The
292 controlled effects included a size-dependent signal, which was modeled using a Gaussian contour pulse
293 that increased in amplitude with increasing shape size (as defined by the shape's average radius) (Fig.9a),
294 and a group-dependent signal, which was modeled similarly, but which was applied to just one of two
295 hypothetical groups (Fig.9b). To isolate and emphasize design flexibility, and to eliminate registration and
296 correspondence as potential sources of error, we controlled both by sampling at 101 evenly distributed

297 angular displacements with respect to the horizontal axis. We considered two MANCOVA possibilities:
298 analysis of the original, unscaled dataset (Fig.9a), and analysis of the scaled / registered dataset (Fig.9b).
299 We applied a single MANCOVA model, which modeled both shape size (i.e., mean shape radius) and
300 group, and which thereby afforded consideration of both (1) size effects, with group effects linearly
301 removed, and (2) group effects, with size effects linearly removed. Size effects for the original, unscaled
302 data naturally showed very large test statistic values at all contour points (Fig.9c). In contrast, size
303 effects for the registered data correctly isolated the modeled size-dependent signal (Fig.9d). Group
304 effects were practically identical for both the original, unscaled data and the registered data (Fig.9e,f),
305 emphasizing the point that MANCOVA can be used to remove size-related effects in lieu of registration.
306 More generally, this analysis shows that the proposed framework is highly flexible, and can be used
307 with arbitrary continuous and categorical independent variables, provided these variables adhere to the
308 requirements of classical linear design modeling. We nevertheless caution readers that the (Fig.9) analyses
309 consider close-to-ideal data, for which registration and correspondence are near-perfectly controlled. For
310 real dataset analysis, both registration and correspondence generally introduce errors that may or not
311 affect the ultimate hypothesis testing results. Results' sensitivity to data processing algorithms and their
312 parameters must be considered in general analyses.

313 **Comparison with landmarking and other methods**

314 The proposed methodology partially overcomes limitations of landmark selection, and the corresponding
315 susceptibility to bias (Arnqvist and Martensson, 1998; Rohlf, 2003; Fruciano, 2016); shape-to-shape
316 landmark identification is often manual and therefore subjective. Algorithmic landmark identification is
317 nevertheless possible (Claes et al., 2011; Strait and Kurtek, 2016), and indeed modern machine learning
318 techniques have been shown to substantially improve landmark detection, with the promise of eliminating
319 landmark-associated subjectivity (Morris, 2003; Young and Maga, 2015; Strait and Kurtek, 2016; Devine
320 et al., 2020). Like automated landmarking, the proposed method can be used with little-to-no subjective
321 intervention, implying generally more repeatable results. Here 'objective' does not necessarily mean
322 'accurate' or 'appropriate'; it simply means that results are expected to be more reproducible than the
323 results from more subjective methods. Determining the accuracy and appropriateness of all methods,
324 including the proposed one, requires substantial empirical effort across a range of data modalities and
325 applications.

326 We also note that the proposed landmark-free approach is just one end of the spectrum, where manual
327 landmark definition is the other, and that a variety of alternative techniques occupy positions between
328 these two extremes. For example, semilandmarks (Mitteroecker and Gunz, 2009) provide an objective way
329 to fill spatial gaps between landmarks, thereby creating a continuous surface. From the perspective of the
330 proposed method, semilandmarks represent the results of piecewise registration over the domain u (Fig.6),
331 or equivalently a hybrid registration method consisting of both algorithmic and manual components
332 (Ramsay and Li, 1998). As there are a plethora of automated techniques for geometrical matching
333 (Holden, 2008), the proposed framework regards these techniques each as objective, substitutable, yet
334 each imperfect components, whose assumptions and parameters could ultimately affect the final results.
335 From this perspective, a second layer of objectivity could be added to the proposed framework, whereby
336 different techniques and/or parameters are iteratively substituted in a sensitivity framework, to objectively
337 discern the numerical stability of the final results, as well as the boundaries of that stability (Pataky et al.,
338 2014).

339 Landmarks and other low-dimensionality representations of shape — including harmonic coefficients
340 from elliptic Fourier analysis (Bonhomme et al., 2014) — embody a second important limitation: a poten-
341 tially over-simplified representation of shape. In the case of landmarks, a danger of over-simplification
342 arises from the Nyquist theorem: under-sampling a continuous process (including the continuous spatial
343 surface of an object) can lead to aliasing, whereby the under-sampled measurement can misrepresent the
344 true characteristics of the underlying object (Nyquist, 1928), and can even reverse statistical interpreta-
345 tions through mechanisms such as regional conflation (Pataky et al., 2008). This latter problem of shape
346 simplification can nevertheless be solved by the use of semi-landmarks (Bookstein, 1997; Adams et al.,
347 2004) which, as argued above, can be regarded as a specific approach to shape registration, implying that
348 semi-landmark approaches could interface easily with the proposed technique.

349 An advantage of the proposed method is processing speed. The current, non-optimized analyses
350 executed in under 2 s, with statistical inference itself requiring well under 100 ms (Table 3). We

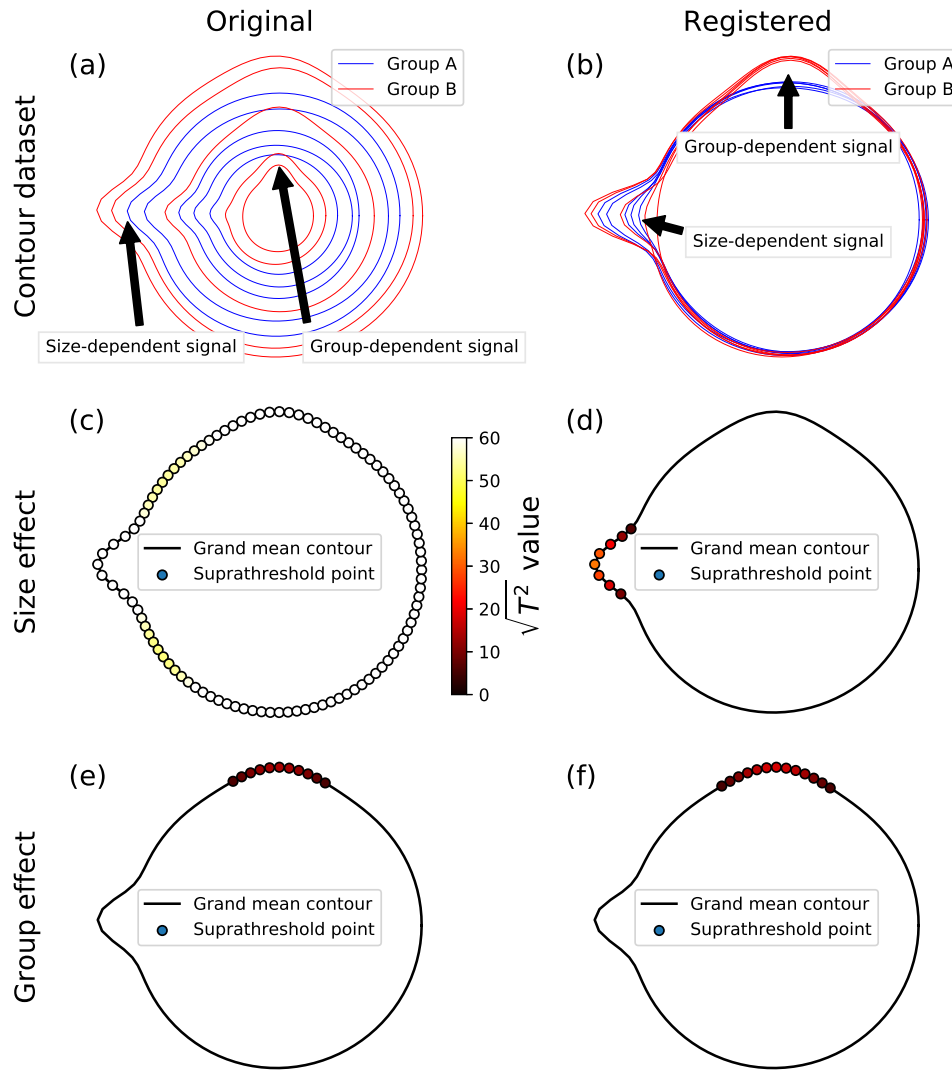


Figure 9. Example MANCOVA using synthetic data; for simplicity, data were generated to have (i) a relatively large signal:noise ratio, and (ii) close-to-perfect correspondence, by sampling at 101 equally spaced angular distances around the contour. (a) The original contour dataset, consisting of five noisy circles for each of two groups, with systematically different mean radii, and also with both group- and size-dependent signal, where ‘size’ was considered to be the mean radius, and where ‘signal’ implies true morphological difference. Note that the size-dependent signal is more easily perceived in panel (a), and that the group-dependent signal is more easily perceived in the next panel. (b) Registered contours. (c,d) Size effects from MANCOVA for the original and registered data; the test statistic is presented as $\sqrt{T^2}$ because a linear T^2 scale would result in imperceivable color differences (i.e., the panel (c) points would be all white, and the points in the other panels would all be close-to-black). (e,f) Group effects from MANCOVA for the original and registered data; note that the (e) and (f) results are similar because MANCOVA accounts for size-related effects in the ‘Original’ data.

351 acknowledge that other data processing steps, including image segmentation and registration for example,
 352 can require substantial effort, so we caution readers that the reported execution speeds do not necessarily
 353 translate to reduced laboratory hours. The primary advantage in our view is instead the promotion of
 354 sensitivity analysis: since the entire data processing chain can be executed relatively rapidly, it would be
 355 possible to systematically adjust algorithm parameters, and even swap algorithms, in a sensitivity loop, to
 356 probe the robustness of particular results.

357 Another advantage of the proposed method is implicit morphological information. The proposed
358 method yields results that are rich in morphological detail (Fig.8) which, much like a highlighted
359 photograph or x-ray image, can be readily interpreted at a glance. Since SPM operates directly on
360 (registered) contours, without reducing the object-of-hypothesis-testing to a single abstract metric (like
361 Procrustes ANOVA), or to a small handful of abstract metrics (like elliptical Fourier analysis), SPM
362 results embody morphological meaning insofar as contours themselves embody morphological meaning.
363 While individual contour points do not necessarily embody meaning, one could argue that the set of all
364 contour points collectively embodies substantial morphological meaning. This perspective is analogous to
365 a pixel-and-image argument. The color of a single pixel is largely irrelevant to the overall interpretation
366 and meaning of an image. Similarly, the test statistic value at a single contour point is itself largely
367 irrelevant to the overall morphological interpretation of SPM results; morphological meaning is instead
368 encapsulated implicitly in the overall excursion set, where 'excursion set' means the set of supra-threshold
369 contour points, like those in Fig.8. Regardless of the quality of morphological meaning, SPM results must
370 be viewed as just one set of results, which may or may not embody useful morphological information,
371 and which should be considered along with other, more explicit morphological methods like Procrustes
372 ANOVA and elliptical Fourier analysis.

373 Considering last specific results from this paper, a particularly unintuitive set of results was observed
374 for the Device8 dataset, for which UV analysis yielded the smallest p value (0.022), and for which no
375 other method yielded significance ($p > 0.2$) (Table 2). This result was likely caused by widespread but
376 relatively small-magnitude mean-shape differences (Fig.8c); since the deformation is widespread it would
377 be detected by a general deformation metric like Procrustes distance, but since the deformation magnitude
378 is relatively small it would not be detected by local contour-point methods like SPM. The interpretation
379 is emphasized in the Flatfish dataset, where general deformations were similarly broadly distributed
380 across the contour, but maximal local deformations were greater (Fig.8e), which yielded significance in
381 all methods (Table 2). Nevertheless, this interpretation appears to be inconsistent with the Horseshoe
382 dataset, which exhibited both large and widely distributed deformation (Fig.8h), but which also failed
383 to yield significant UV results (Table 2). Nevertheless, this apparent consistency may be resolved by
384 considering the large variability in the Horseshoe dataset, particularly at the selected landmarks (Fig.2h).
385 To more completely resolve such apparent inconsistencies, and more generally to understand the nature of
386 landmark- vs. contour-based methods, it would be necessary to consider individual contour points, their
387 deformations, and their covariances.

388 **Generalization to 3D analysis**

389 While this paper was limited to 2D analysis, it should be noted that the proposed analysis framework
390 (Fig.1d) can be readily extendable to the morphological analysis of 3D surfaces. Similar to the unwrapping
391 of 2D contours onto a 1D domain u (Fig.6), 3D surfaces can be unwrapped onto a 2D domain uv Fig.10,
392 and methods like SPM (Friston et al., 2007) can be used to conduct domain-level hypothesis testing
393 regarding these unwrapped data. This domain-wide testing is possible due to the underlying model of
394 domain-level variance, which SPM models as smooth, Gaussian random fields, and which can be extended
395 to arbitrarily high-dimensional domains with arbitrary geometry (Adler and Taylor, 2007). For the current
396 paper involving 2D shapes, the (flattened) domain is one-dimensional, and the dependent variable is a
397 two-component position vector; that is, a two-component position is defined at all locations u along the
398 contour. Similarly, for 3D surfaces, the (flattened) domain is two-dimensional and the dependent variable
399 is a three-component position vector, where position is defined at all locations uv across the surface. A
400 variety of computational tools exist for 3D geometry flattening (e.g. Dale et al., 1999; Sawhney and Crane,
401 2017), so 3D implementations of the proposed method could presumably proceed in a fully automated
402 manner.

403 **Limitations**

404 The proposed mass-multivariate framework (Fig.1d) has a number of limitations. The most severe of
405 these is sensitivity to algorithmic specifics. For example, simply by randomly changing the order of the
406 points, it is possible to yield qualitatively different results (Fig.11). Systematic, random variations of
407 point ordering would be necessary for assessment of the results' sensitivity, but in our view this would
408 be insufficient because ultimate results may also be sensitive to other particulars including, for example,
409 specific parameter values used in contour parameterization, registration, and correspondence algorithms.
410 In other words, one should regard the results as potentially sensitive to all data processing steps, and not

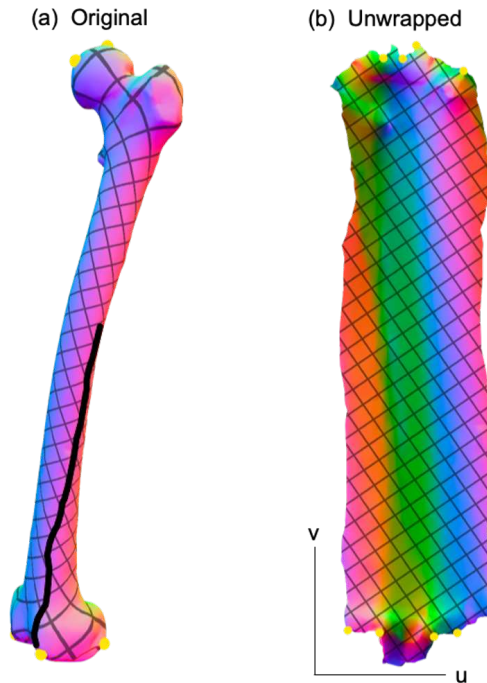


Figure 10. Example 3D surface unwrapping. (a) Original 3D geometry. (b) Unwrapped geometry; this is a 2D parametric (UV) representation of the original geometry. Colors represent changes in surface normal direction. The thick black line in panel (a) represents a seam along which the 3D geometry is cut so that it can be flattened into a 2D shape. Unwrapping was performed here using boundary first flattening (Sawhney and Crane, 2017).

411 just to point ordering. The current paragraph considers just one example (point ordering) as a potential
 412 source of sensitivity concern. In (Fig.11), the qualitative change in results can be attributed to a minor
 413 shift in point correspondence (Fig.11a-b), which created a small shift in pointwise covariance, but a
 414 shift that was large enough to alter the hypothesis rejection decision at $\alpha = 0.05$. That is, point-specific
 415 covariance is direction dependent, so small changes in point-deformation direction can yield qualitative
 416 changes in test statistics (Pataky et al., 2014). Nevertheless, we observed this type of sensitivity to random
 417 point ordering only occasionally, with most randomizations resulting in qualitatively similar results. Also,
 418 in most cases we noticed that probability results, while variable, were generally stable. The problem
 419 only emerged qualitatively when that variability spanned $\alpha=0.05$, as depicted in Fig.11). This problem
 420 of probability value variability (Halsey et al., 2015) partially reflects a weakness of classical hypothesis
 421 testing, which has a binary interpretation of continuous probability. We acknowledge that we did not
 422 systematically conduct sensitivity testing, and also that each stage of processing involves a variety of
 423 components or parameters that could be subjected to sensitivity analysis. Comprehensive consideration of
 424 this sensitivity would require a large research effort, so we leave this for future work.

425 The datasets and analyses presented in this paper also have limitations. We analyzed shapes from
 426 just one database (Carlier et al., 2016) and, for each dataset, we selected only ten shapes for analysis,
 427 and only conducted two-sample tests. While we do not expect analysis of datasets from other databases
 428 to appreciably affect this paper's messages, we acknowledge that analyses of relatively small samples,
 429 and just one simple experimental design, fully exposes neither the advantages nor disadvantages of the
 430 proposed analysis framework. We selected just ten shapes for each dataset primarily to emphasize that
 431 the proposed parametric procedure is sufficiently sensitive to detect morphological effects for small
 432 sample sizes. The specific ten shapes were selected in an *ad hoc* manner to emphasize particular concepts
 433 including, for example: interpretation agreement between the proposed and landmark methods' results,
 434 and the opposite: interpretation disagreement. Since these datasets were selected in an *ad hoc* manner,
 435 from a single database, and with only two-sample analyses, the reader is left to judge the relevance of
 436 these results to other datasets and experimental designs.

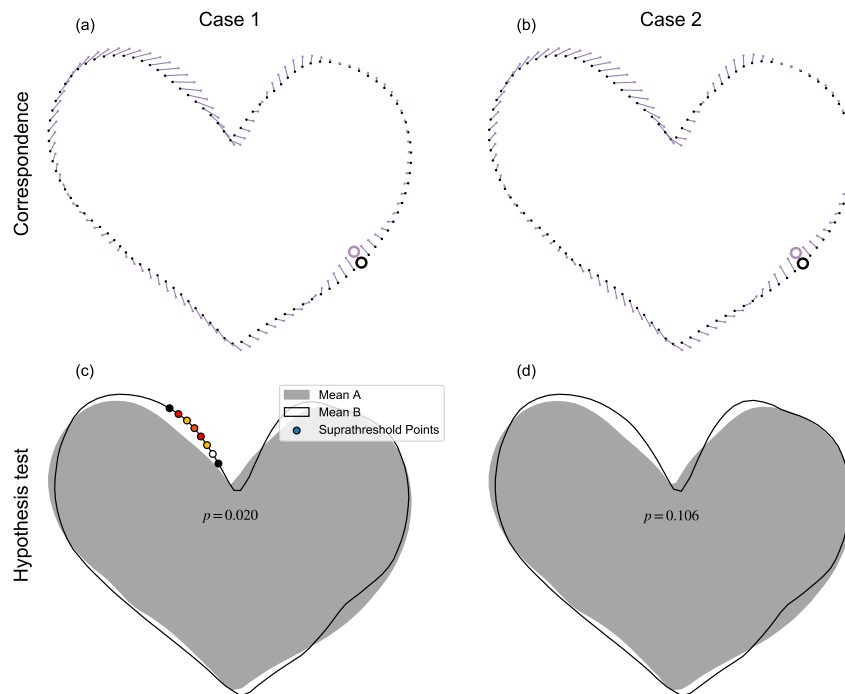


Figure 11. Example processing sensitivity. Case 1 depicts the result reported in Fig.8g. Case 2 depicts the results after point re-shuffling (i.e., a new random points order, see Fig.5a), then re-application of the processing chain depicted in Fig.1d. Note: results for Case 1 were qualitatively replicated for most random re-shufflings, but approximately 1 in 20 re-shufflings yielded qualitatively different results, like those depicted for Case 2.

CONCLUSIONS

This paper demonstrates that parametric hypothesis testing can be conducted at the whole-contour level with suitably high statistical power for the analysis of even relatively small samples of 2D shapes ($N = 10$). We describe a general framework for automated, landmark-free hypothesis testing of 2D contour shapes, but this paper implements just one realization of that framework. The main advantages of the proposed framework are that results are calculated quickly (<2 s in this paper), and yield morphologically rich results in an easy-to-interpret manner. Since innumerable realizations of the proposed framework are possible through algorithm and parameter substitution at each stage in the proposed data processing chain, sensitivity analysis may generally be required for robust statistical conclusions.

ACKNOWLEDGMENTS

This work was supported by Kiban B Grant 17H02151 from the Japan Society for the Promotion of Science. There was no additional external funding received for this study.

REFERENCES

- Adams, D. C. and Otárola-Castillo, E. (2013). Geomorph: an R package for the collection and analysis of geometric morphometric shape data. *Methods in Ecology and Evolution*, 4(4):393–399.
- Adams, D. C., Rohlf, F. J., and Slice, D. E. (2004). Geometric morphometrics: ten years of progress following the 'revolution'. *Italian Journal of Zoology*, 71(1):5–16.
- Adams, D. C., Rohlf, F. J., and Slice, D. E. (2013). A field comes of age: geometric morphometrics in the 21st century. *Hystrix*, 24(1):7.
- Adler, R. J. and Taylor, J. E. (2007). *Random Fields and Geometry*. Springer-Verlag.
- Anaconda (2020). Anaconda Software Distribution version 3-6.10.

- 458 Anderson, M. and Braak, C. T. (2003). Permutation tests for multi-factorial analysis of variance. *Journal*
459 *of Statistical Computation and Simulation*, 73(2):85–113.
- 460 Arnqvist, G. and Martensson, T. (1998). Measurement error in geometric morphometrics: empirical
461 strategies to assess and reduce its impact on measures of shape. *Acta Zoologica Academiae Scientiarum*
462 *Hungaricae*, 44(1-2):73–96.
- 463 Bingol, O. R. and Krishnamurthy, A. (2019). NURBS-Python: An open-source object-oriented NURBS
464 modeling framework in Python. *SoftwareX*, 9:85–94.
- 465 Bonhomme, V., Picq, S., Gaucherel, C., and Claude, J. (2014). Momocs: Outline Analysis Using R.
466 *Journal of Statistical Software*, 56(13):1–25.
- 467 Bookstein, F. L. (1996). Biometrics, biomathematics and the morphometric synthesis. *Bulletin of*
468 *Mathematical Biology*, 58(2):313.
- 469 Bookstein, F. L. (1997). Landmark methods for forms without landmarks: morphometrics of group
470 differences in outline shape. *Medical Image Analysis*, 1(3):225–243.
- 471 Brombin, C. and Salmaso, L. (2009). Multi-aspect permutation tests in shape analysis with small sample
472 size. *Computational Statistics & Data Analysis*, 53(12):3921–3931.
- 473 Carrier, A., Leonard, K., Hahmann, S., Morin, G., and Collins, M. (2016). The 2D shape structure dataset:
474 a user annotated open access database. *Computers & Graphics*, 58:23–30.
- 475 Casanovas-Vilar, I. and Van Dam, J. (2013). Conservatism and adaptability during squirrel radiation:
476 what is mandible shape telling us? *PLoS One*, 8(4):e61298.
- 477 Chung, M. K., Worsley, K. J., Nacewicz, B. M., Dalton, K. M., and Davidson, R. J. (2010). General
478 multivariate linear modeling of surface shapes using SurfStat. *NeuroImage*, 53(2):491–505.
- 479 Claes, P., Walters, M., Vandermeulen, D., and Clement, J. G. (2011). Spatially-dense 3d facial asymmetry
480 assessment in both typical and disordered growth. *Journal of anatomy*, 219(4):444–455.
- 481 Claude, J. (2013). Log-Shape Ratios, Procrustes Superimposition, Elliptic Fourier Analysis: Three
482 Worked Examples in R. *Hystrix, the Italian Journal of Mammalogy*, 24(1):94–102.
- 483 Collyer, M. L., Sekora, D. J., and Adams, D. C. (2015). A method for analysis of phenotypic change for
484 phenotypes described by high-dimensional data. *Heredity*, pages 1–9.
- 485 Corti, M. (1993). Geometric morphometrics: an extension of the revolution. *Trends in Ecology &*
486 *Evolution*, 8(8):302.
- 487 Cullen, J. A. and Marshall, C. D. (2019). Do sharks exhibit heterodonty by tooth position and over
488 ontogeny? a comparison using elliptic fourier analysis. *Journal of Morphology*, 280(5):687–700.
- 489 Da Costa, L. d. F. and Cesar, R. M. (2000). *Shape Analysis and Classification: Theory and Practice*. CRC
490 Press, Inc.
- 491 Dale, A. M., Fischl, B., and Sereno, M. I. (1999). Cortical surface-based analysis: I. segmentation and
492 surface reconstruction. *Neuroimage*, 9(2):179–194.
- 493 Devine, J., Aponte, J. D., Katz, D. C., Liu, W., Lo Vercio, L. D., Forkert, N. D., Marcucio, R., Percival,
494 C. J., and Hallgrímsson, B. (2020). A Registration and Deep Learning Approach to Automated
495 Landmark Detection for Geometric Morphometrics. *Evolutionary Biology*, 47(3):246–259.
- 496 Dumont, M., Wall, C. E., Botton-Divet, L., Goswami, A., Peigné, S., and Fabre, A.-C. (2016). Do
497 functional demands associated with locomotor habitat, diet, and activity pattern drive skull shape
498 evolution in musteloid carnivorans? *Biological Journal of the Linnean Society*, 117(4):858–878.
- 499 Friston, K. J., Ashburner, J. T., Kiebel, S. J., Nichols, T. E., and Penny, W. D. (2007). *Statistical Parametric*
500 *Mapping: The Analysis of Functional Brain Images*. Elsevier, London.
- 501 Fruciano, C. (2016). Measurement error in geometric morphometrics. *Development Genes and Evolution*,
502 226(3):1–20.
- 503 Fu, A. L., Hammerschlag, N., Lauder, G. V., Wilga, C. D., Kuo, C.-Y., and Irschick, D. J. (2016).
504 Ontogeny of head and caudal fin shape of an apex marine predator: The tiger shark (*Galeocerdo cuvier*).
505 *Journal of Morphology*, 277(5):556–564.
- 506 Goodall, C. (1991). Procrustes methods in the statistical analysis of shape. *Journal of the Royal Statistical*
507 *Society: Series B (Methodological)*, 53(2):285–321.
- 508 Gower, J. C. (1975). Generalized procrustes analysis. *Psychometrika*, 40(1):33–51.
- 509 Hallgrímsson, B., Percival, C. J., Green, R., Young, N. M., Mio, W., and Marcucio, R. (2015). Morpho-
510 metrics, 3D Imaging, and Craniofacial Development. In *Craniofacial Development*, pages 561–597.
511 Elsevier.
- 512 Halsey, L. G., Curran-Everett, D., Vowler, S. L., and Drummond, G. B. (2015). The fickle P value

513 generates irreproducible results. *Nature Methods*, 12(3):179–185.

514 Hill, J. J., Puttick, M. N., Stubbs, T. L., Rayfield, E. J., and Donoghue, P. C. (2018). Evolution of jaw
515 disparity in fishes. *Palaeontology*, 61(6):847–854.

516 Holden, M. (2008). A review of geometric transformations for nonrigid body registration. *IEEE*
517 *Transactions on Medical Imaging*, 27(1):111–128.

518 Kendall, D. G. (1977). The diffusion of shape. *Advances in applied probability*, 9(3):428–430.

519 Kendall, D. G. (1984). Shape manifolds, procrustean metrics, and complex projective spaces. *Bulletin of*
520 *the London mathematical society*, 16(2):81–121.

521 Kendall, D. G. (1985). Exact distributions for shapes of random triangles in convex sets. *Advances in*
522 *Applied Probability*, pages 308–329.

523 Kent, J. T. (1994). The complex bingham distribution and shape analysis. *Journal of the Royal Statistical*
524 *Society: Series B (Methodological)*, 56(2):285–299.

525 Klingenberg, C. P. and McIntyre, G. S. (1998). Geometric morphometrics of developmental instability:
526 analyzing patterns of fluctuating asymmetry with procrustes methods. *Evolution*, 52(5):1363–1375.

527 Kurnianggoro, L., Wahyono, and Jo, K.-H. (2018). A survey of 2D shape representation: Methods,
528 evaluations, and future research directions. *Neurocomputing*, 300:1–16.

529 Loy, A., Busilacchi, S., Costa, C., Ferlin, L., and Cataudella, S. (2000). Comparing geometric morpho-
530 metrics and outline fitting methods to monitor fish shape variability of *diplodus puntazzo* (teleostea:
531 Sparidae). *Aquacultural Engineering*, 21(4):271–283.

532 Mitteroecker, P. and Gunz, P. (2009). Advances in geometric morphometrics. *Evolutionary Biology*,
533 36(2):235–247.

534 Mitteroecker, P., Gunz, P., Bernhard, M., Schaefer, K., and Bookstein, F. L. (2004). Comparison of cranial
535 ontogenetic trajectories among great apes and humans. *Journal of Human Evolution*, 46(6):679–698.

536 Morgan, C. C. (2009). Geometric morphometrics of the scapula of south american caviomorph rodents
537 (rodentia: Hystricognathi): form, function and phylogeny. *Mammalian Biology*, 74(6):497–506.

538 Morris, B. (2003). The components of the wired spanning forest are recurrent. *Probability theory and*
539 *related fields*, 125(2):259–265.

540 Murphy-Chutorian, E. and Trivedi, M. M. (2008). Head pose estimation in computer vision: A survey.
541 *IEEE transactions on Pattern Analysis and Machine Intelligence*, 31(4):607–626.

542 Myronenko, A. and Song, X. (2010). Point set registration: coherent point drift. *IEEE Transactions on*
543 *Pattern Analysis and Machine Intelligence*, 32(12):2262–2275.

544 Nichols, T. and Holmes, A. (2002). Nonparametric permutation tests for functional neuroimaging: a
545 primer with examples. *Human Brain Mapping*, 15(1):1–25.

546 Nyquist, H. (1928). Certain topics in telegraph transmission theory. *Transactions of the American Institute*
547 *of Electrical Engineers*, 47(2):617–644.

548 Page, C. E. and Cooper, N. (2017). Morphological convergence in ‘river dolphin’ skulls. *PeerJ*, 5:e4090.

549 Pataky, T. C. (2012). One-dimensional statistical parametric mapping in Python. *Computer Methods in*
550 *Biomechanics and Biomedical Engineering*, 15(3):295–301.

551 Pataky, T. C., Caravaggi, P., Savage, R., and Crompton, R. (2008). Regional peak plantar pressures are
552 highly sensitive to region boundary definitions. *Journal of Biomechanics*, 41(12):2772–2775.

553 Pataky, T. C., Robinson, M. A., Vanrenterghem, J., Savage, R., Bates, K. T., and Crompton, R. H. (2014).
554 Vector field statistics for objective center-of-pressure trajectory analysis during gait, with evidence of
555 scalar sensitivity to small coordinate system rotations. *Gait and Posture*, 40(1):255–258.

556 Pedoia, V., Samaan, M. A., Inamdar, G., Gallo, M. C., Souza, R. B., and Majumdar, S. (2017). Study of
557 the interactions between proximal femur 3d bone shape, cartilage health, and biomechanics in patients
558 with hip Osteoarthritis. *Journal of Orthopaedic Research*, 25(1):114–12.

559 R Core Team (2019). *R: A Language and Environment for Statistical Computing*. R Foundation for
560 Statistical Computing, Vienna, Austria.

561 Ramsay, J. O. and Li, X. (1998). Curve registration. *Journal of the Royal Statistical Society Series B*.

562 Renaud, S., Michaux, J., Schmidt, D. N., Aguilar, J. P., Mein, P., and Auffray, J. C. (2005). Morphological
563 evolution, ecological diversification and climate change in rodents. *Proceedings of the Royal Society B:*
564 *Biological Sciences*, 272(1563):609–617.

565 Rohlf, F. J. (1990). Fitting curves to outlines. In *Proceedings of the Michigan morphometrics workshop*,
566 number 2, pages 167–177. The University of Michigan Museum of Zoology Ann Arbor Michigan.

567 Rohlf, F. J. (1999). Shape statistics: Procrustes superimpositions and tangent spaces. *Journal of*

568 *Classification*, 16(2):197–223.

569 Rohlf, F. J. (2000a). On the use of shape spaces to compare morphometric methods. *Hystrix-the Italian*
570 *Journal of Mammalogy*, 11(1).

571 Rohlf, F. J. (2000b). Statistical power comparisons among alternative morphometric methods. *American*
572 *Journal of Physical Anthropology: The Official Publication of the American Association of Physical*
573 *Anthropologists*, 111(4):463–478.

574 Rohlf, F. J. (2003). Bias and error in estimates of mean shape in geometric morphometrics. *Journal of*
575 *Human Evolution*, 44(6):665–683.

576 Rohlf, F. J. and Marcus, L. F. (1993). A revolution morphometrics. *Trends in ecology & evolution*,
577 8(4):129–132.

578 Sawhney, R. and Crane, K. (2017). Boundary first flattening. *ACM Transactions on Graphics (ToG)*,
579 37(1):1–14.

580 Singleton, M. (2015). Functional geometric morphometric analysis of masticatory system ontogeny in
581 papionin primates. *The Anatomical Record*, 298(1):48–63.

582 Slice, D. E. (2007). Geometric morphometrics. *Annual Review of Anthropology*, 36:261–281.

583 Stayton, C. T. (2005). Morphological evolution of the lizard skull: a geometric morphometrics survey.
584 *Journal of Morphology*, 263(1):47–59.

585 Strait, J. and Kurtz, S. (2016). Bayesian model-based automatic landmark detection for planar curves.
586 In *Proceedings of the IEEE Conference on Computer Vision and Pattern Recognition Workshops*, pages
587 86–94.

588 Taylor, J. E. and Worsley, K. J. (2008). Random fields of multivariate test statistics, with applications to
589 shape analysis. *Annals of Statistics*, 36(1):1–27.

590 Terhune, C. E., Cooke, S. B., and Otárola-Castillo, E. (2015). Form and function in the platyrrhine skull:
591 A three-dimensional analysis of dental and tmj morphology. *The Anatomical Record*, 298(1):29–47.

592 Toro-Ibacache, V., Muñoz, V. Z., and O’Higgins, P. (2016). The relationship between skull morphol-
593 ogy, masticatory muscle force and cranial skeletal deformation during biting. *Annals of Anatomy-*
594 *Anatomischer Anzeiger*, 203:59–68.

595 van Rossum, G. (2019). The Python Library Reference Release 3.6.10.

596 Wuhrer, S., Shu, C., and Xi, P. (2011). Landmark-free posture invariant human shape correspondence.
597 *The Visual Computer*, 27(9):843–852.

598 Young, R. and Maga, A. M. (2015). Performance of single and multi-atlas based automated landmarking
599 methods compared to expert annotations in volumetric microCT datasets of mouse mandibles. *Frontiers*
600 *in Zoology*, pages 1–12.

601 Zelditch, M. L., Swiderski, D. L., and Sheets, H. D. (2012). *Geometric Morphometrics for Biologists: A*
602 *Primer*. Academic Press.

603 Zhang, D. and Lu, G. (2004). Review of shape representation and description techniques. *Pattern*
604 *Recognition*, 37(1):1–19.